

Article

Effect of Complexation with *Closo*-Decaborate Anion on Photophysical Properties of Copolyfluorenes Containing Dicyanophenanthrene Units in the Main Chain

Anton A. Yakimanskiy ¹, Ksenia I. Kaskevich ¹, Tatiana G. Chulkova ¹, Elena L. Krasnopeeveva ^{1,*}, Serguei V. Savilov ^{2,3}, Vera V. Voinova ³, Nikolay K. Neumolotov ³, Andrey P. Zhdanov ³, Anastasia V. Rogova ⁴, Felix N. Tomilin ^{4,5}, Konstantin Yu. Zhizhin ³ and Alexander V. Yakimansky ¹

- ¹ Institute of Macromolecular Compounds, RAS, Bolshoi Prospect of Vasilyevsky Island 31, Saint Petersburg 199004, Russia; yakimanski@gmail.com (A.A.Y.); kaskevich-ksenia@yandex.ru (K.I.K.); tgc@mail.ru (T.G.C.); yakimansky@yahoo.com (A.V.Y.)
- ² Department of Chemistry, Lomonosov Moscow State University, Moscow 119991, Russia; savilov@mail.ru
- ³ Kurnakov Institute of General and Inorganic Chemistry, RAS, Moscow 119991, Russia; veravoinova@rx24.ru (V.V.V.); neumolotovn@gmail.com (N.K.N.); zh_dots@mail.ru (A.P.Z.); zhizhin@igic.ras.ru (K.Y.Z.)
- ⁴ Kirensky Institute of Physics, Federal Research Center KSC SB RAS, Krasnoyarsk 660036, Russia; arogoval927@gmail.com (A.V.R.); felixnt@gmail.com (F.N.T.)
- ⁵ Laboratory for Digital Controlled Drugs and Theranostics, Federal Research Center KSC SB RAS, Krasnoyarsk 660041, Russia
- * Correspondence: opeeveva@gmail.com; Tel.: +7-812-3237407



Citation: Yakimanskiy, A.A.; Kaskevich, K.I.; Chulkova, T.G.; Krasnopeeveva, E.L.; Savilov, S.V.; Voinova, V.V.; Neumolotov, N.K.; Zhdanov, A.P.; Rogova, A.V.; Tomilin, F.N.; et al. Effect of Complexation with *Closo*-Decaborate Anion on Photophysical Properties of Copolyfluorenes Containing Dicyanophenanthrene Units in the Main Chain. *Micro* **2023**, *3*, 930–940. <https://doi.org/10.3390/micro3040063>

Academic Editor: Zlatan Denchev

Received: 14 October 2023

Revised: 24 November 2023

Accepted: 28 November 2023

Published: 30 November 2023



Copyright: © 2023 by the authors. Licensee MDPI, Basel, Switzerland. This article is an open access article distributed under the terms and conditions of the Creative Commons Attribution (CC BY) license (<https://creativecommons.org/licenses/by/4.0/>).

Abstract: The functionalization of copolyfluorenes containing dicyanophenanthrene units by *closo*-decaborate anion is described. Target copolyfluorenes were analyzed using SEM, UV-vis, luminescence, NMR, and Fourier-transform infrared (FTIR) spectroscopy. The effect of complexation with the *closo*-decaborate anion on the photophysical properties was studied both experimentally and theoretically. The PL data indicate an efficient charge transfer from fluorene to the dicyanophenanthrene units coordinated to the *closo*-decaborate. The coordination of *closo*-decaborate clusters to the nitrile groups of copolyfluorenes provides an important route to new materials for sensors and light-emitting devices while, at the same time, serving as a platform for further study of the nature of boron clusters.

Keywords: CAM-B3LYP; charge transfer; copolyfluorene; energy transfer; hole-electron distribution; nitrilium derivatives of *closo*-decaborate anions; lambda-diagnostic; luminescence; phenanthrene-9,10-dicarbonitrile; TD-DFT

1. Introduction

Copolyfluorenes (CPFs) are very important for the practical advanced applications of optoelectronic and photovoltaic devices, as well as biomedicine, due to their luminescence and charge mobility properties. The donor–acceptor architecture of CPFs with π -conjugated units (D– π –A copolymers) has attracted much attention, owing to its charge (CT) and energy transfer (ET) effects [1–5]. This strategy has been widely applied to design high-efficiency light-emitting polymers. In the donor–acceptor copolymer system, the proper electron-deficient group, in addition to the electron-rich fluorene unit, are critical factors for obtaining excellent copolymer performance. The electron-deficient cyano-substituted aromatic groups are effective and widely used acceptors, as they provide excellent electron injection/transport, high photoluminescence, and thermal stability. Measures such as incorporating an electron transport unit into the main chain were taken to balance the carrier transport to improve the EL performance. The coordination of boron cluster anions to nitriles leads to an increase in the electrophilicity of the carbon atom of the cyano

group. As a result, the boron clusters can affect the electron-withdrawing properties of coordinated cyano groups, as well as the luminescence of functionalized copolyfluorenes with cyano-substituted units. CT and ET processes may have an important impact on the performance of optoelectronic devices and, therefore, deserve careful study. The efficiencies of CT and ET depend very sensitively on the donor–acceptor distance, on the energy-level (or band) offsets, and on the local dielectric and electrostatic environment. On the one hand, Förster-type energy transfer, mediated by relatively long-range (up to several nm) dipole–dipole coupling, is now engineered in a variety of light-harvesting devices and distance sensors [6]. Charge transfer, on the other hand, is a much shorter-range process (about 1 nm) that plays a key role in a number of molecular and solid state systems, and is at the origin of the operation of photodetectors and solar cells [7].

Based on the 9,10-dicyanophenanthrene electron-deficient acceptor, together with the frequently used derivative of fluorene as the donor (9,9-dioctylfluorene), a series of copolymers were synthesized and functionalized by the *closo*-decaborate anion. *Closo*-decaborate functionalized copolyfluorenes with different contents of 9,10-dicyanophenanthrene units were studied both photophysically and using theoretical calculations.

2. Materials and Methods

All reagents and starting materials were purchased from commercial suppliers and used without further purification. Solvents were purified by standard methods.

The polycondensation reactions were performed in the CEM Discover LabMate single-mode microwave reactor (CEM Corporation, Matthews, NC, USA) at a radiation frequency of 2.45 GHz and a maximum generator power of 300 W. The temperature of synthesis was controlled using an infrared sensor placed under the reaction vessel. The reaction parameters (temperature, power, time, stirring rate) were set manually.

Polymer films were prepared on an Ossila spin coater and dried or heated in a UT-4620 drying chamber. The CPF films were formed by spin coating on the glass from polymer solutions in toluene (200–220 μ L). The toluene solution concentration was 10 mg/mL.

NMR spectra were recorded on a Bruker AVANCE-400 SB (400 MHz) spectrometer (Bruker, Billerica, MA, USA) at room temperature. The UV-visible absorption spectra were recorded on a Shimadzu UV-1900 spectrophotometer (Shimadzu, Kyoto, Japan). Photoluminescence spectra were measured using an RF-6000 spectrofluorophotometer (Shimadzu, Kyoto, Japan). The absorption and emission spectra of the films were measured immediately before heating and then after exposure for 4 h in the drying chamber at 80 °C and a high-ventilation mode. FT-IR spectra were recorded on a Shimadzu IR Affinity-1S spectrometer (Shimadzu, Kyoto, Japan) using a Quest single-reflection ATR accessory (Specac, Fort Washington, PA, USA), KRS-5 prism, 7800–400 cm^{-1} range (ISP Optics, Irvington, NY, USA).

2.1. Synthesis of CPFs

CPFs containing 0.5, 2.5, and 5% of 9,10-dicyanophenanthrene units (PFCN0.5, PFCN2.5, and PFCN5, respectively) were synthesized via a Suzuki–Miyaura cross-coupling reaction according to a procedure described previously [8]. Their structures were confirmed by ^1H NMR and FT-IR spectroscopy. The molecular mass characteristics of the copolyfluorenes are presented in the Supplementary Materials Table S1.

2.2. Synthesis of CPFs Derivatives of the Closo-Decaborate Anion

Method A: PFCN x (30 mg for $x = 0.5$ or 20 mg for $x = 2.5$ and 5) and $(\text{NBu}_4)[\text{B}_{10}\text{H}_{11}]$ (1.1 eq. to the cyano groups contained in the copolymer; 0.4, 1.1, and 2.2 mg, respectively) were dissolved in 3 mL of anhydrous 1,2-dichloroethane and purged with argon for 15 min. The resulting solution was heated in the sealed tube for 6 h at 80 °C with stirring. The solution was dried on a rotary evaporator and the residual pale yellow solid was stored in a drying chamber.

^1H NMR and FT-IR spectral data for the synthesized compounds (PFCN0.5+B, PFCN2.5+B, and PFCN5+B) are given in the Supplementary Materials Table S2, Figure S1.

Method B: PFCN2.5 (7 mg) and $(\text{Ph}_4\text{P})[\text{B}_{10}\text{H}_{11}]$ (5 mg, 10^{-2} mmol) were mixed, followed by the addition of 3 mL of dichloromethane. The reaction mixture was purged with argon and stirred in a sealed tube for 4 h at 45 °C. Subsequently, the solvent was removed under reduced pressure on a rotary evaporator. The target product (PFCN2.5+B') was extracted with toluene, concentrated on a rotary evaporator, and dried under a vacuum.

^1H NMR, $^{11}\text{B}\{^1\text{H}\}$ NMR, and FT-IR spectra for PFCN2.5+B' are presented in the Supplementary Materials Figures S2–S4.

2.3. Scanning Electron Microscopy (SEM)

The specimens were imaged by SEM using a JEOL JSM 6490 LV instrument. The energy of the primary electrons was 10 keV and the current was varied within the range of 2–40 pA. The focal length of the electron beam was varied in the range of 9 to 14 mm. The accelerating voltages were commonly set to 20 kV. The morphology of the samples was determined in the backscattered electron mode in low-vacuum mode. For elemental microanalysis of the sample surface (EDS), an energy dispersive system, EX-54 175 JMH (JEOL), was used. For this study, samples were placed on conductive tape and secured to the sample holder using it. To ensure electrical conductivity, a layer of gold was sputtered on top.

2.4. Calculation Methods

The atomic and electronic structure, electron density distribution, absorption and luminescence spectra, and oscillator strengths for the ionic forms of the phenanthrene molecules, including the solvent, were calculated using density functional theory (DFT). Calculations were performed for 3,6-di(4-methylphenyl)phenanthrene-9,10-dicarbonitrile coordinated to one (PFCN-B1, Figure 1a) or two *closo*-decaborate anion clusters, $\text{B}_{10}\text{H}_9^-$ (PFCN-B2, Figure 1c,d). The SMD model [9] was used to account for the solvent (chloroform). All calculations were performed with the CAM-B3LYP functional [10]. It has been shown previously [8] that CAM-B3LYP better describes the phenanthrene molecule. To choose the most appropriate basis set, a comparative analysis of theoretically calculated spectra and experimental data was performed for each structure ($\text{B}_{10}\text{H}_9^-$, PFCN-B1, PFCN-B2). The 6-31+(p,d) basis was used for the *closo*-decaborate anion $\text{B}_{10}\text{H}_9^-$. The choice of basis was motivated by the fact that the $\text{B}_{10}\text{H}_9^-$ cluster is charged. For the calculation of the ionic forms of PFCN-B1 and PFCN-B2, the 6-31+(p,d) basis was chosen, which includes polarization and diffusion functions. Since further excited state geometries were calculated, the choice of the basis is an important step. In general, the SMD/CAM-B3LYP/6-31+(p,d) level of the DFT theory was preferred by the totality of the data. Absorption and luminescence spectra for all phenanthrene molecules (models) were obtained using TD theory [11]. The calculations were performed in the program GAMESS [12].

The calculations were performed as follows. (1) The $\text{B}_{10}\text{H}_9^-$ anion was constructed (Figure 1a). The geometry optimization in the ground and excited states was carried out in a vacuum and taking into account the solvent (chloroform). The spectral properties of the cluster were then calculated. (2) Next, the effect of $\text{B}_{10}\text{H}_9^-$ on the phenanthrene molecule was investigated (Figure 1b). For this purpose, one or two nitrile groups of 3,6-di(4-methylphenyl)phenanthrene-9,10-dicarbonitrile were occupied by boron cluster anions (PFCN-B1 and PFCN-B2, Figure 1c,d). Geometry optimization in the ground and excited states was performed. Absorption and luminescence spectra were calculated using the TD/CAM-B3LYP level of theory.

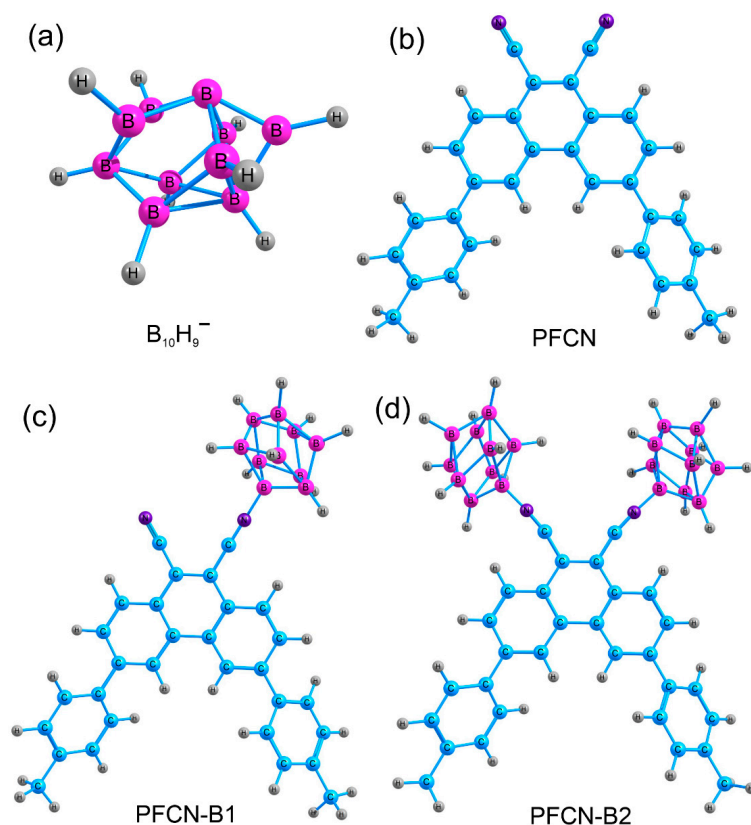


Figure 1. Atomic structures of the calculated molecules. (a) $B_{10}H_9^-$ anion cluster; (b) 3,6-di(4-methylphenyl)phenanthrene-9,10-dicarbonitrile (PFCN); (c) monofunctionalized 3,6-di(4-methylphenyl)phenanthrene-9,10-dicarbonitrile by closo-decaborate anion (PFCN-B1); (d) difunctionalized 3,6-di(4-methylphenyl)phenanthrene-9,10-dicarbonitrile by closo-decaborate anion (PFCN-B2). C, H, N, and B atoms are colored blue, gray, purple, and pink, respectively.

The criterion for separating local transitions from charge transfer and Rydberg transitions is the analysis of the Λ parameter [10]. A value of $0.45 \leq \Lambda \leq 0.89$ indicates local excitations, which are characterized by a large overlap of molecular orbitals. In contrast, Rydberg transitions are characterized by a value in the range of $0.08 \leq \Lambda \leq 0.27$, which is much smaller and indicates minimal spatial overlap between the occupied and virtual orbitals [10]. In calculations, it was found that at absorption, the Λ parameter was in the range of $0.14 < \Lambda < 0.41$; thus, both local and charge transfer transitions are possible in these molecules. In addition, other types of diagnostics can be used, such as the Δr parameter, which allows the study of excited states [13]. This parameter is a characteristic of the hole–electron distribution, which is an additional criterion for the analysis of the excited state of molecules. Calculated results of the hole–electron distribution for PFCN-B1 and PFCN-B2 molecules were performed in the program Multiwfn [14].

3. Results and Discussion

3.1. Synthesis of Closo-Decaborate Nitrilium Derivatives of CPFs with Dicyanophenanthrene Units

Currently, methods for providing derivatives of the general formula $[B_{10}H_9NCR]^-$ with simple alkyl and aryl substituents have been reliably developed [15,16]. However, polymeric nitrilium derivatives with boron clusters have not yet been obtained. In this work, closo-decaborate nitrilium derivatives of copolyfluorenes with 9,10-dicyanophenanthrene units (PFCN_x+B) were synthesized according to the reaction scheme presented in Figure 2.

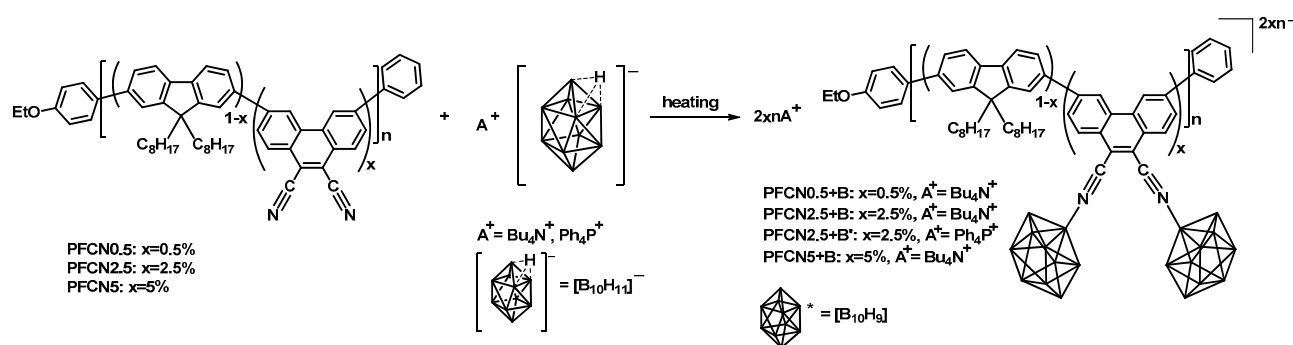


Figure 2. Synthesis of *closo*-decaborate nitrilium derivatives of copolyfluorenes with 9,10-dicyanophenanthrene units (PFCN x +B, PFCN2.5+B').

The reaction between the fluorene-based copolymer containing cyano groups and the *closo*-decaborate salt in its protonated form, $(\text{Bu}_4\text{N})[\text{B}_{10}\text{H}_{11}]$ or $(\text{Ph}_4\text{P})[\text{B}_{10}\text{H}_{11}]$, was conducted under conditions standard for the electrophile-induced nucleophilic substitution (EINS) mechanism [17]. An excess of *closo*-decaborate was used to make sure all the CN-groups in the copolymer were reacted. The reaction was monitored via ^{11}B , ^1H NMR spectroscopy and IR spectroscopy. The most informative method was IR spectroscopy, which indicated the presence of B-H bonds in the reaction product ($2400\text{--}2600\text{ cm}^{-1}$), as well as CN-B ($2350\text{--}2400\text{ cm}^{-1}$) (Supplementary Materials Table S2, Figure S4). These values are consistent with data obtained for the addition products of low-molecular-weight nitriles [18]. Due to the low concentration of cyano groups in the copolymer, NMR spectroscopy was less informative. In the ^1H NMR spectra of PFCN x +B, signals of tetrabutylammonium protons in the range from 1.0 to 3.3 ppm can clearly be seen (Supplementary Materials Table S2, Figure S1). In the ^1H NMR spectrum of PFCN2.5+B', the protons of the phenyl groups of the PPh_4^+ cation overlap with the aromatic protons of the copolymer in the region of 7.5–8.0 ppm. The protons associated with the boron atoms in the cluster appear in a broad range of 0 to 2 ppm and are not distinguishable due to the low concentration of the cluster in the substance and overlapping (Supplementary Materials Figure S2). On the other hand, ^{11}B NMR provides significant information. Although it seems hard to correlate signals with specific boron atoms, the overall spectrum shape qualitatively indicates the reaction progression. The absence of signals from the apical position of the original *closo*-decaborate in the system; (2) and the presence of a nitrile derivative of the *closo*-decaborate anion. The morphology of the as-prepared PFCN2.5+B' sample was analyzed by SEM (Figure 3). According to the SEM data, the material possess a layered structure from laminar fragments with a size of 1–5 microns. Energy dispersive analysis data indicate the presence of phosphorus from the triphenylphosphonium cation (Supplementary Materials Figure S5).

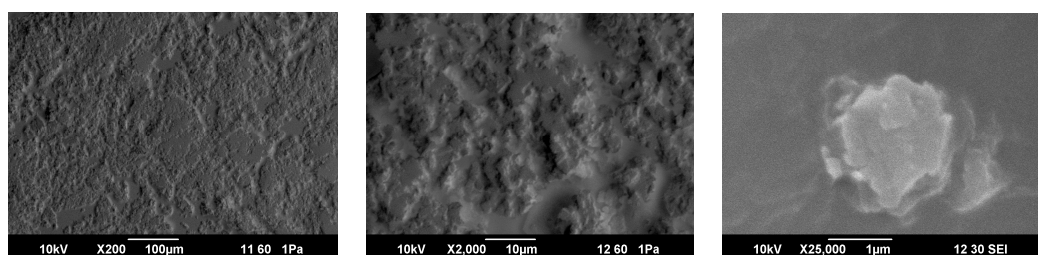


Figure 3. SEM images of PFCN2.5+B'.

The surface has a granular-fibrous morphology, typical for films of many polymers formed by the spin-coating method.

3.2. Photophysical Properties of Modified CPFs

The UV–vis absorption spectra of the PFCN_x+B polymers were measured in films (Supplementary Materials, Table S3). The most intense band at ca. 385 nm in the spectra corresponds to the π – π^* transition in the fluorene fragments [19–22]. The same band is observed in the UV–vis spectra of the PFCN_x polymers. In the polymer functionalized with boron clusters (PFCN_x+B), the band at ca. 395 nm begins to appear. Also, the shoulder at ca. 430 nm becomes more intense and redshifted compared to the non-functionalized polymer.

In the photoluminescence spectra of the PFCN_x+B films (Supplementary Materials Table S3), an intensive band at 500–530 nm is observed. In general, the addition of boron clusters to the cyano groups of the copolymer leads to an increase in luminescence intensity (Supplementary Materials Figure S6). Additionally, the fluorescence quantum yields of PFCN5 and PFCN5+B were measured in a chloroform solution using quinine sulfate dihydrate as a reference. The quantum yield for PFCN5+B (74%) was slightly higher than that for PFCN5 (70%). These data indicate a significant compensation of the electron-withdrawing properties of the boron cluster by the negative charge localized on it.

Probably, the observed Stokes shifts (Supplementary Materials Table S3) are related to the degree of structural reorganization of the two-fold C_{2v} -symmetrical luminophoric dicyanophenanthrene moiety with boron clusters in the copolymers, the intramolecular charge–transfer characteristics of the copolymers in the film state, or the intermolecular charge–transfer between the *closo*-decaborate nitrilium units and fluorene moieties in the copolymers.

3.3. Theoretical Calculations

The absorption and emission maxima for PFCN-B1 and PFCN-B2 calculated by the TD/SMD/CAM-B3LYP/6-31+(p,d) method are presented in Table 1. The calculation of the absorption spectra of the *closo*-decaborate cluster (the $S_0 \rightarrow S_2$ transition with an oscillator strength of 0.004 is 424 nm) shows that the *closo*-decaborate cluster can influence the appearance of the shoulder in the experimental spectrum in the range of 425–450 nm (Supplementary Materials, Table S3). At the same time, the calculated oscillator strengths of the transitions in the emission spectra turned out to be low.

Table 1. Calculation of the spectral properties of PFCN-B1 and PFCN-B2 at the TD/SMD/CAM-B3LYP/6-31+(p,d) level of the theory.

Absorption			Emission		
Transition	λ_{abs} , nm	f	Transition	λ_{flu} , nm	f
PFCN-B1					
$S_0 \rightarrow S_1$	387 (HOMO-1, 88% *) \rightarrow LUMO	0.78	$S_1 \rightarrow S_0$	423 LUMO \rightarrow (HOMO-3, 51%; HOMO-7, 28%)	0.89
$S_0 \rightarrow S_2$	352 (HOMO-3, 17%; HOMO-4, 18%; HOMO-6, 23% HOMO-7, 19%) \rightarrow LUMO	0.34	$S_2 \rightarrow S_0$	372 LUMO \rightarrow (HOMO-3, 21%; HOMO-5, 18%; HOMO-7, 51%)	0.34
MO	HOMO	LUMO	$S_3 \rightarrow S_0$	347 LUMO \rightarrow (HOMO-5, 92%)	0.11
E_{MO}	–6.33	–1.91			
ΔE	4.42				
PFCN-B2					
$S_0 \rightarrow S_1$	412 (HOMO-4, 89%) \rightarrow LUMO	0.84	$S_1 \rightarrow S_0$	563 LUMO \rightarrow (HOMO-1, 81%)	0.47
$S_0 \rightarrow S_2$	376 (HOMO-5, 56%; HOMO-10, 19%) \rightarrow LUMO	0.53	$S_2 \rightarrow S_0$	433 LUMO \rightarrow (HOMO-4, 89%)	0.68
MO	HOMO	LUMO	$S_3 \rightarrow S_0$	396 LUMO \rightarrow (HOMO-5, 74%)	0.27
E_{MO}	–6.04	–1.88			
ΔE	4.16				

λ_{abs} , λ_{flu} , and f —maximum absorption, emission wavelengths (nm), and oscillator strength; MO—molecular orbital; E_{MO} —energy of molecular orbitals, eV; ΔE —energy gap between HOMO and LUMO, eV; * contributing transitions; other contributions are less than 1%.

Upon the introduction of boron clusters ($B_{10}H_9$) into dicyanophenanthrene, an increase in light absorption intensity and splitting of one peak at 380 nm into two (at 380 nm and 397 nm) is experimentally observed. Two maximum absorption spectra at 387 nm and 352 nm are observed for compound PFCN-B1, whereas 412 nm and 376 nm are observed for PFCN-B2 (Table 1). The introduction of a cluster ($B_{10}H_9$) to the cyano group at the position 9 of phenanthrene shifts the theoretical maximum of the absorption spectrum to the red region (by 28 nm), whereas the introduction of the second *closo*-decaborate cluster shifts it more to the long-wavelength region (by 35 nm) relative to PFCN (phenanthrene without the boron cluster). Thus, there is a correspondence between the experimental values of the transition energies in the absorption spectrum and the energy corresponding to the position of the maximum of the calculated absorption spectrum for PFCN-B1 and PFCN-B2 (Figure 4).

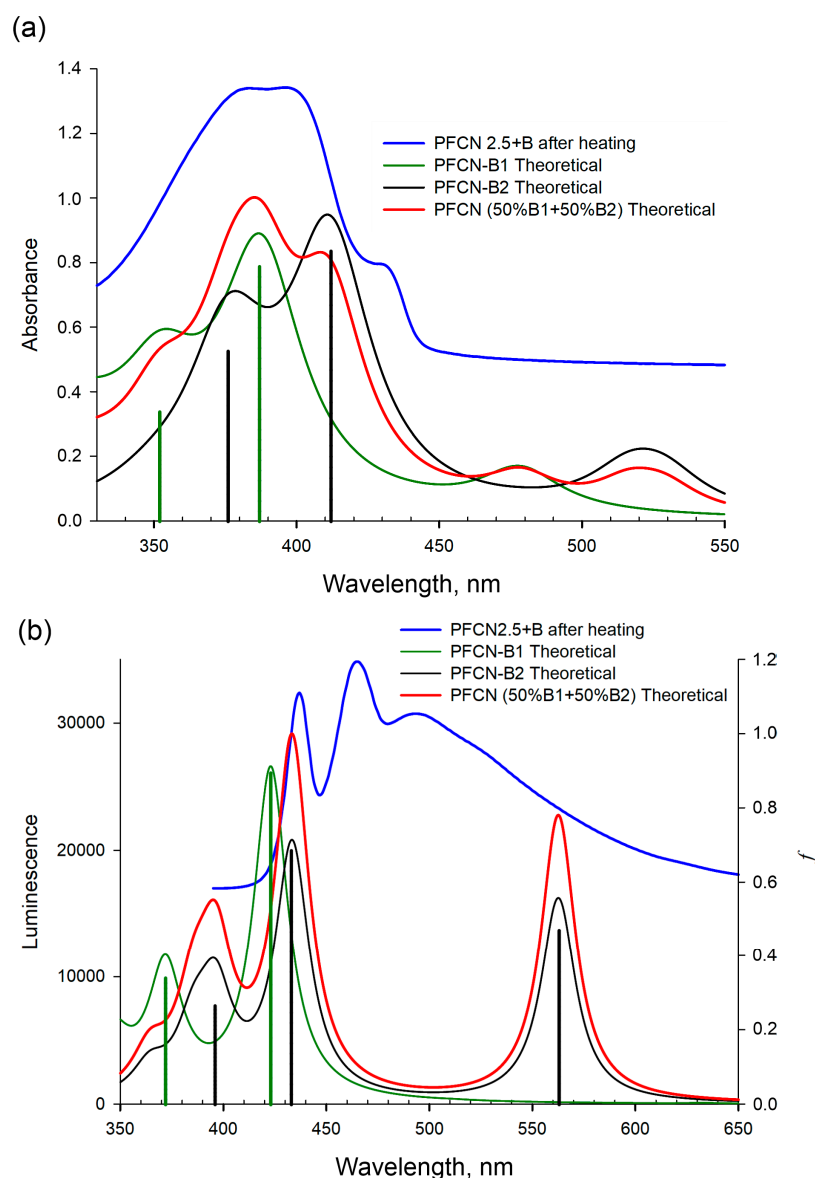


Figure 4. Experimental absorption and luminescence spectra (in film) and theoretical spectra for PFCN-B1 and PFCN-B2 structures calculated by TD/SMD/CAM-B3LYP/6-31+(p,d). (a) Absorption spectrum. (b) Luminescence spectrum. Blue line—the experiment. Green vertical bar—theoretical electronic transition for PFCN-B1. Green line—spectral model. Black vertical bar—theoretical electronic transition for PFCN-B2. Black line—spectral model. Red line—theoretical spectral model for a mixture of 50% PFCN-B1 and 50% PFCN-B2.

A similar pattern is observed in the emission spectra. The addition of one boron cluster ($B_{10}H_9$) results in a shift (of 5 nm) to the red region (423 nm, Figure 4) relative to PFCN (417 nm [8]). The addition of the second boron cluster ($B_{10}H_9$) shifts the maximum of the emission spectrum to 433 nm and an additional peak appears in the red region (at 563 nm). Comparing the experimental and calculated data, a shift of the theoretical emission spectra to the blue region is observed relative to the experiment. Several emission bands are observed in the experimental luminescence spectrum, which may indicate that different parts of the molecule are independently involved in this process.

In the large molecules, there may be transitions with charge transfer to different parts of the molecule [23]. In this case, when the modeling excites state transitions, more TD-DFT transitions are used to account for the contributions of different MOs to the excited transitions that belong to different parts of the molecule. All the transitions obtained in the calculations (Figure S7) occur from the LUMO, but to different MOs (HOMO-2, HOMO-5, etc.). Therefore, the transitions from the excited state to the ground state occur on different segments of the molecule from the same excited level (Figure S7). To interpret such a complex emission spectrum, it is sufficient to consider two transitions from the excited state to the ground state for the PFCN-B1 molecule and three transitions for the PFCN-B2 molecule. It is clear that the $B_{10}H_9$ cluster is actively involved in these processes.

According to the calculations, the highest occupied molecular orbitals, HOMO-2, HOMO-7 and HOMO-4, and HOMO-5 for PFCN-B1 and PFCN-B2, respectively, describe the $S_0 \rightarrow S_1$, $S_0 \rightarrow S_2$ transitions (Figure S8). In the absorption spectra, the electron density of LUMO is localized on the dicyanophenanthrene group for both PFCN-B1 and PFCN-B2 molecules. The charge transfer transition to the LUMO from the higher occupied orbitals, HOMO-2, HOMO-7 (PFCN-B1) and HOMO-4, and HOMO-5 (PFCN-B2), leads to the formation of Franck–Condon states, S_1 and S_2 , respectively. The $S_0 \rightarrow S_1$ transition for PFCN-B1 has a large HOMO-1 contribution of 88% and high oscillator strength (0.78); the electron density is located on the dicyanophenanthrene, *p*-tolyl, and $B_{10}H_9$ fragments; and the $S_0 \rightarrow S_2$ transition consists of contributions from different molecular orbitals, such as HOMO-3 (17%), HOMO-4 (18%), HOMO-6 (23%), and HOMO-7 (19%). Thus, different regions of the molecule are responsible for this transition. For the PFCN-B2 structure, the molecular orbital HOMO-4 (89% contribution) is responsible for the $S_0 \rightarrow S_1$ transition. The calculated transition has high oscillator strength (0.84) and the electron density is located on the dicyanophenanthrene, *p*-tolyl, and $B_{10}H_9$ fragments. The $S_0 \rightarrow S_2$ transition consists of different contributions from molecular orbitals, such as HOMO-5 (56%) and HOMO-10 (18%), with the electron density largely located on the $B_{10}H_9$ cluster. This diversity suggests a complex behavior of the electron density under excitation, which is related to the extended conjugated sites and the influence of the $B_{10}H_9$ cluster on the chromophore group.

The molecular orbitals that had the largest contribution to the corresponding luminescence maxima are summarized in Figure S7. The calculated electronic transitions in the luminescence spectrum of PFCN-B1 include five orbitals: HOMO-2, HOMO-3, HOMO-5, HOMO-7, and LUMO (Table 1, Figure S7a). The first S_1 - S_0 transition manifests at different parts of the molecule and is described by LUMO \rightarrow HOMO-3, LUMO \rightarrow HOMO-5, and LUMO \rightarrow HOMO-7 transitions with different contributions (21%, 18%, and 51%, respectively); the S_2 - S_0 transition is described by a pair of LUMO and HOMO-2 orbitals (Table 1, Figure S7a). The S_2 - S_0 transition has high oscillator strength, with a large HOMO-2 contribution of 92% (the electron density is on the dicyanophenanthrene groups, Figure S7a). For the molecule for PFCN-B2 (Table 1, Figure S7b), the first S_1 - S_0 transition is from LUMO to HOMO-5. The second and third S_2 - S_0 and S_3 - S_0 are described by LUMO \rightarrow HOMO-4 and LUMO \rightarrow HOMO-1 orbital pairs with different contributions (89% and 74%, respectively), that is, the emission spectra of the modified copolymers demonstrate a significant energy transfer from fluorene segments to dicyanophenanthrene groups coordinated to the $B_{10}H_9$ boron clusters.

The analysis of the hole–electron distribution is summarized in Table S4 and Figures S10 and S11. The hole–electron contributions to each part of the molecules were

studied and a fragment-based heat map was constructed. For the PFCN-B1 molecule, the system was divided into four fragments (Figure S10), and for the PFCN-B2 molecule, the system was divided into five fragments (Figure S11). The data obtained show that for the PFCN-B1 molecule, for the $S_1 \rightarrow S_0$ transition, 85.25% of electrons are located on the fourth fragment (dicyanophenanthrene, Figure S10), whereas 26.72% and 24.76% of holes are located on fragment 3 ($B_{10}H_9$ cluster) and fragment 1 (p-tolyl), respectively. The degree of hole–electron overlap on the fourth fragment is 56%. This means that the electron transfer during the excitation process is from the third and first fragment to the fourth fragment. For the $S_2 \rightarrow S_0$ transition, 85.38% of electrons and 44.36% of holes are located on the fourth fragment (dicyanophenanthrene, Figure S10) and 41.08% of holes are located on the third fragment ($B_{10}H_9$ cluster). This means that the excited electrons mainly come from fragment number three to fragment four. For the PFCN-B2 molecule for the $S_1 \rightarrow S_0$ and $S_3 \rightarrow S_0$ transitions, the electrons are located on fragment five (more than 80%, dicyanophenanthrene, Figure S11) and the holes are located on fragment three ($B_{10}H_9$ fragment). The excited electrons come mainly from fragment three, with most of them transferring to fragment five (dicyanophenanthrene). For the $S_2 \rightarrow S_0$ transition, 85.31% of electrons and 45.92% of holes are located on fragment five (dicyanophenanthrene, Figure S11) and the holes are located on fragments three and four ($B_{10}H_9$ clusters), more than 20% per fragment. Thus, the excited electrons come from fragment five and three and remain on dicyanophenanthrene. All these data are well confirmed by the D, S_r , and t indices (Table S4).

All calculated structures show a slight difference in geometry with the addition of the boron cluster. The bond lengths and angles $\alpha 1-3$, $\beta 1-3$, $\gamma 1-3$, $\varphi 1-3$ for PFCN, PFCN-B1, and PFCN-B2, respectively, were used to describe the change in the geometry of the molecules upon the addition of the substituent $B_{10}H_9$ (Supplementary Materials Figure S9a–f). When $B_{10}H_9$ is added, there is a change in the angle $\beta 1-3$ when two $B_{10}H_9$ are added and the angles become less than 180° , but in the excited state, $\gamma 3$ and $\varphi 3$ are closer to 180° . All of this leads to the fact that the presence of two $B_{10}H_9$ must be accompanied by a bathochromic shift.

4. Conclusions

In summary, the first example of functionalization of CPFs containing 9,10-dicyanophenanthrene units by *closo*-decaborate anion was achieved. The reaction between the fluorene-based copolymer and *closo*-decaborate proceeds through the EINS mechanism.

The introduction of the $B_{10}H_9$ boron cluster affects the photophysical properties of copolyfluorenes. When the boron clusters are introduced into the dicyanophenanthrene unit, a splitting of one peak at 380 nm into two (at 380 nm and 397 nm) is experimentally observed. The PL emission spectra of the functionalized copolymers show significant energy transfer from fluorene segments to the dicyanophenanthrene units coordinated to the $B_{10}H_9$ boron clusters. These data are in good agreement with theoretical calculations. Our theoretical calculations show that the charge transfer takes place in the polymer chain from fluorene to the *closo*-decaborate nitrilium phenanthrene moieties.

Supplementary Materials: The following supporting information can be downloaded at: <https://www.mdpi.com/article/10.3390/micro3040063/s1>, Figure S1: 1H NMR spectra of compounds (PFCN0.5+B, PFCN2.5+B, and PFCN5+B) in $CDCl_3$; Figure S2: 1H NMR spectrum of PFCN2.5+B' in $CDCl_3$; Figure S3: $^{11}B\{^1H\}$ NMR spectrum of PFCN2.5+B' in $CDCl_3$; Figure S4: FT-IR spectra of PFCN2.5 (top) and PFCN2.5+B' (bottom); Figure S5: EDS for PFCN2.5+B'; Figure S6: PL spectra of PFCN2.5, PFCN2.5+B, PFCN2.5 after heating at $80^\circ C$ for 4 h, and PFCN2.5+B after heating at $80^\circ C$ for 4 h in films; Figure S7: Transition scheme and molecular orbitals in the excited state of molecules. (a) Molecular orbitals of the PFCN-B1. (b) Molecular orbitals of the PFCN-B2 molecule. Transition maxima in the luminescence spectrum according to Table 1. Energy of molecular orbitals in eV. The f is the oscillator strength. Maximum contributions of orbitals involved in this transition are given in percent (%). The inset shows the experimental luminescence spectrum. Figure S8: Molecular orbitals for the ground state of PFCN-B1 and PFCN-B2. (a) Molecular orbitals for the $S_0 \rightarrow S_1$ transition of PFCN-B1. (b) Molecular orbitals for the $S_0 \rightarrow S_2$ transition of PFCN-B1. (c) Molecular orbitals for the $S_0 \rightarrow S_1$ transition of PFCN-B2. (d) Molecular orbitals for the $S_0 \rightarrow S_2$ transition of PFCN-B2.

The MOs according to Table 1, with the maximum contribution, are indicated. Figure S9: Atomic structure of the calculated molecules in the ground and excited states. Bond lengths (Å) and angles characterizing the change in spatial structure upon introduction of the boron cluster ($B_{10}H_9^-$) in the ground and excited states for different phenanthrene compounds. (a) PFCN geometry in the ground state. (b) PFCN geometry in the excited state. (c) PFCN-B1 geometry in the ground state. (d) PFCN-B1 geometry in the excited state. (e) PFCN-B2 geometry in the ground state. (f) PFCN-B2 geometry in the excited state. Figure S10: The PFCN-B1 molecular fragment electron excitation process analyzed by the hole–electron and interfragment charge transfer (IFCT) method. Contribution of different fragments of PFCN-B1 to the electron orbitals $S_1 \rightarrow S_0$ and $S_2 \rightarrow S_0$ states (%). Holes and electrons are given in blue and green iso-surfaces. Figure S11: The PFCN-B2 molecular fragments electron excitation process analyzed by the IFCT method. Contribution of different fragments of PFCN-B1 to the electron orbitals $S_1 \rightarrow S_0$, $S_2 \rightarrow S_0$, $S_3 \rightarrow S_0$ states (%). Holes and electrons are given in blue and green iso-surfaces. Table S1: Molecular mass characteristics of copolyfluorenes. Table S2: FT-IR and 1H NMR selected data for synthesized compounds. Table S3: UV-Vis and fluorescence spectral data for CPFs films. Table S4: The calculated results of the excited states for PFCN-B1 and PFCN-B2, including the characteristics of the hole–electron distribution.

Author Contributions: Conceptualization, A.P.Z., K.Y.Z., F.N.T., T.G.C. and A.V.Y.; methodology, A.P.Z., F.N.T., T.G.C., S.V.S. and A.V.Y.; formal analysis, A.P.Z., K.Y.Z., F.N.T., T.G.C. and A.V.Y.; investigation, A.A.Y., K.I.K., V.V.V., N.K.N., A.V.R., S.V.S. and F.N.T.; writing—original draft preparation, A.P.Z., T.G.C., F.N.T., S.V.S. and A.V.Y.; writing—review and editing, T.G.C., E.L.K., K.Y.Z., F.N.T. and A.V.Y.; supervision, T.G.C., A.P.Z., K.Y.Z., F.N.T. and A.V.Y.; project administration, T.G.C., E.L.K. and A.V.Y.; funding acquisition, A.V.Y. All authors have read and agreed to the published version of the manuscript.

Funding: This work was supported by the Russian Science Foundation, grant no. 23-43-00060.

Institutional Review Board Statement: Not applicable.

Informed Consent Statement: Not applicable.

Data Availability Statement: Data is contained within the article or Supplementary Materials.

Conflicts of Interest: The authors declare no conflict of interest.

References

1. Grimsdale, A.C.; Chan, K.L.; Martin, R.E.; Jokisz, P.G.; Holmes, A.B. Synthesis of Light-Emitting Conjugated Polymers for Applications in Electroluminescent Devices. *Chem. Rev.* **2009**, *109*, 897–1091. [[CrossRef](#)] [[PubMed](#)]
2. Beaujuge, P.M.; Reynolds, J.R. Color Control in π -Conjugated Organic Polymers for Use in Electrochromic Devices. *Chem. Rev.* **2010**, *110*, 268–320. [[CrossRef](#)] [[PubMed](#)]
3. Khasbaatar, A.; Xu, Z.; Lee, J.-H.; Campillo-Alvarado, G.; Hwang, C.; Onusaitis, B.N.; Diao, Y. From Solution to Thin Film: Molecular Assembly of π -Conjugated Systems and Impact on (Opto)Electronic Properties. *Chem. Rev.* **2023**, *123*, 8395–8487. [[CrossRef](#)] [[PubMed](#)]
4. Kim, K.; Inagaki, Y.; Kanehashi, S.; Ogino, K. Synthesis of Polyfluorene-Polytriarylamine Block Copolymers with Light-Emitting Benzothiadiazole Moieties: Effect of Chromophore Location on Electroluminescent Properties. *Polym. J.* **2017**, *49*, 721–728. [[CrossRef](#)]
5. Bezgin Carbas, B. Fluorene Based Electrochromic Conjugated Polymers: A Review. *Polymer* **2022**, *254*, 125040. [[CrossRef](#)]
6. Guzelurk, B.; Demir, H.V. Near-Field Energy Transfer Using Nanoemitters For Optoelectronics. *Adv. Funct. Mater.* **2016**, *26*, 8158–8177. [[CrossRef](#)]
7. May, V.; Kühn, O. *Charge and Energy Transfer Dynamics in Molecular Systems*; John Wiley & Sons, Inc.: New York, NY, USA, 2011; p. 562.
8. Yakimanskiy, A.A.; Kaskevich, K.I.; Zhukova, E.V.; Berezin, I.A.; Litvinova, L.S.; Chulkova, T.G.; Lypenko, D.A.; Dmitriev, A.V.; Pozin, S.I.; Nekrasova, N.V.; et al. Synthesis, Photo- and Electroluminescence of New Polyfluorene Copolymers Containing Dicyanostilbene and 9,10-Dicyanophenanthrene in the Main Chain. *Materials* **2023**, *16*, 5592. [[CrossRef](#)] [[PubMed](#)]
9. Tomasi, J.; Mennucci, B.; Cammi, R. Quantum Mechanical Continuum Solvation Models. *Chem. Rev.* **2005**, *105*, 2999–3093. [[CrossRef](#)]
10. Peach, M.J.G.; Benfield, P.; Helgaker, T.; Tozer, D.J. Excitation Energies in Density Functional Theory: An Evaluation and a Diagnostic Test. *J. Chem. Phys.* **2008**, *128*, 044118. [[CrossRef](#)]
11. Marques, M.A.L.; Gross, E.K.U. Time-Dependent Density Functional Theory. *Annu. Rev. Phys. Chem.* **2004**, *55*, 427–455. [[CrossRef](#)]
12. Schmidt, M.W.; Baldridge, K.K.; Boatz, J.A.; Elbert, S.T.; Gordon, M.S.; Jensen, J.H.; Koseki, S.; Matsunaga, N.; Nguyen, K.A.; Su, S.; et al. General Atomic and Molecular Electronic Structure System. *J. Comput. Chem.* **1993**, *14*, 1347–1363. [[CrossRef](#)]

13. Guido, C.A.; Cortona, P.; Mennucci, B.; Adamo, C. On the Metric of Charge Transfer Molecular Excitations: A Simple Chemical Descriptor. *J. Chem. Theory Comput.* **2013**, *9*, 3118–3126. [[CrossRef](#)] [[PubMed](#)]
14. Lu, T.; Chen, F. Multiwfn: A Multifunctional Wavefunction Analyzer. *J. Comput. Chem.* **2012**, *33*, 580–592. [[CrossRef](#)] [[PubMed](#)]
15. Nelyubin, A.V.; Klyukin, I.N.; Zhdanov, A.P.; Grigor'ev, M.S.; Zhizhin, K.Y.; Kuznetsov, N.T. Synthesis of Nitrile Derivatives of the Closo-Decaborate and Closo-Dodecaborate Anions [BnHn–1NCR]–(n = 10, 12) by a Microwave Method. *Russ. J. Inorg. Chem.* **2021**, *66*, 139–145. [[CrossRef](#)]
16. Stogniy, M.Y.; Erokhina, S.A.; Sivaev, I.B.; Bregadze, V.I. Nitrilium Derivatives of Polyhedral Boron Compounds (Boranes, Carboranes, Metallocarboranes): Synthesis and Reactivity. *Phosphorus Sulfur Silicon Relat. Elem.* **2019**, *194*, 983–988. [[CrossRef](#)]
17. Frank, R.; Adhikari, A.K.; Auer, H.; Hey-Hawkins, E. Electrophile-Induced Nucleophilic Substitution of the Nido-Dicarbaundecaborate Anion Nido-7,8-C2b9h12 by Conjugated Heterodienes. *Chem. A Eur. J.* **2014**, *20*, 1440–1446. [[CrossRef](#)]
18. Ezhov, A.V.; Vyal'ba, F.Y.; Kluykin, I.N.; Zhdanova, K.A.; Bragina, N.A.; Zhdanov, A.P.; Zhizhin, K.Y.; Mironov, A.F.; Kuznetsov, N.T. Synthesis of New Bioinorganic Systems Based on Nitrilium Derivatives of Closo-Decaborate Anion and Meso-Arylporphyrins with Pendant Amino Groups. *Macroheterocycles* **2017**, *10*, 505–509. [[CrossRef](#)]
19. Klärner, G.; Lee, J.I.; Davey, M.H.; Miller, R.D. Exciton Migration and Trapping in Copolymers Based on Dialkylfluorenes. *Adv. Mater.* **1999**, *11*, 115–119. [[CrossRef](#)]
20. Zhang, Q.; Chi, L.; Hai, G.; Fang, Y.; Li, X.; Xia, R.; Huang, W.; Gu, E. An Easy Approach to Control β -Phase Formation in PFO Films for Optimized Emission Properties. *Molecules* **2017**, *22*, 315. [[CrossRef](#)]
21. Zhao, S.; Liang, J.; Guo, T.; Wang, Y.; Chen, X.; Fu, D.; Xiong, J.; Ying, L.; Yang, W.; Peng, J.; et al. Formation of Poly(9,9-Dioctylfluorene) β -Phase by Incorporating Aromatic Moiety in Side Chain. *Org. Electron.* **2016**, *38*, 130–138. [[CrossRef](#)]
22. Perevedentsev, A.; Chander, N.; Kim, J.S.; Bradley, D.D.C. Spectroscopic Properties of Poly(9,9-Dioctylfluorene) Thin Films Possessing Varied Fractions of β -Phase Chain Segments: Enhanced Photoluminescence Efficiency via Conformation Structuring. *J. Polym. Sci. Part B Polym. Phys.* **2016**, *54*, 1995–2006. [[CrossRef](#)] [[PubMed](#)]
23. Loukova, G.V.; Milov, A.A.; Vasiliev, V.P.; Minkin, V.I. Frontier Orbitals and Ligand-to-Metal Charge Transfer Electronic Transitions in d⁰-Metal Complexes. *High Energy Chem.* **2017**, *51*, 333–337. [[CrossRef](#)]

Disclaimer/Publisher's Note: The statements, opinions and data contained in all publications are solely those of the individual author(s) and contributor(s) and not of MDPI and/or the editor(s). MDPI and/or the editor(s) disclaim responsibility for any injury to people or property resulting from any ideas, methods, instructions or products referred to in the content.